Electronic Structure of $HMn(CO)_5$, $H_2Fe(CO)_4$, and $HCo(CO)_4$: Molecular Orbitals, Transition Energies, and Photoactive States

Charles J. Eyermann and Alice Chung-Phillips*

Contribution from the Department of Chemistry, Miami University, Oxford, Ohio 45056.
Received October 18, 1983

Abstract: The self-consistent-field Xα scattered-wave (SCF–Xα–SW) method has been used to investigate the electronic structure of the mononuclear transition metal carbonyl hydride complexes $HMn(CO)_5$, $H_2Fe(CO)_4$, and $HCo(CO)_4$. A summary of the relative energies and individual characteristics of the ground-state valence molecular orbitals (MOs) is presented. The upper valence ionization potentials, obtained via transition-state calculations, are shown to be in quantitative agreement with experimental photoelectron spectra. These calculations also confirm the highest occupied MO to be metal 3d in character. For the study of excited states, Xα–SW transition-state calculations of lower electronic transition energies for $HMn(CO)_5$ and $HCo(CO)_4$ have been carried out and compared with observed electronic spectra. Furthermore, as model studies for the photochemistry of similar monohydride and dihydride complexes, the Xα–SW virtual orbitals of the three complexes are used to postulate possible photoactive states. Results are in accord with the observed photochemistry, including the concerted photodissociation of H_2 from $H_2Fe(CO)_4$.

In the vibrant area of homogeneous catalysis, a considerable effort has been made to explore and understand the chemistry of transition-metal hydride complexes.[1] To date, most of these investigations have focused on their structure and reactivity; only a few theoretical studies on the electronic structure[2-7] have been undertaken. Indeed, there is still a lack of rigorous quantum mechanical description of the metal–hydrogen interaction essential to the interpretation of the observed chemistry.

Recently, the photochemistry of transition-metal hydrides has commanded much attention because of its importance in homogeneous organometallic chemistry. A noteworthy example[8] is the photochemical generation, from transition-metal dihydrides, of complexes capable of activating alkane C–H bonds. In seeking a link between the observed photochemical behavior of some hydrides and their electronic structure, we have carried out systematic self-consistent-field (SCF) Xα scattered-wave (SW) calculations[9] on the electronic structure of some mononuclear and dinuclear hydride complexes.[10,11]

In this work, we have selected $HMn(CO)_5$, $H_2Fe(CO)_4$, and $HCo(CO)_4$ as models for mononuclear transition-metal carbonyl hydrides. These complexes are chemically important; for example, $H_2Fe(CO)_4$ has been postulated as an intermediate in the catalysis of the industrially important water-gas shift reaction,[12] and $HCo(CO)_4$ has been implicated as a catalytic precursor in the hydroformylation of alkenes.[13] More importantly, sufficient quantitative experimental data on these complexes are available to gauge our theoretical calculations. A gas-phase diffraction study has revealed the respective idealized geometries of C_{4v}, C_{2v}, and C_{3v} symmetry.[14] The photoelectron spectra are well-known.[15-17] The UV–vis spectra of $HMn(CO)_5$ and $HCo(CO)_4$ have been reported.[18,19] Furthermore, the products of UV photolyses of all three complexes have been under scrutiny with the matrix-isolation technique.[19-24] The latter studies have already given an impetus to the identification of the excited states involved in these photochemical reactions.[25,26]

For this theoretical investigation, we have two objectives: to provide the first thorough study of the ground-state electronic structure of these complexes, including their ionization potentials (IPs) and low-energy electronic transitions; and, of more direct interest, to use the ground-state molecular orbitals (MOs) and the virtual orbitals of these complexes to postulate photoactive excited states which may be important in the photochemistry of related monohydride and dihydride complexes.

Methodology

In order to formulate plausible photoactive excited states and to discuss the photochemistry of each of the chosen complexes, it is necessary that the ordering of the calculated energy levels for the upper valence MOs and low-lying virtual orbitals be sufficiently correct. In particular, the characters of the highest occupied MO (HOMO) and the lowest unoccupied MO (LUMO) must be firmly established. We now present the reasons for our

(1) For general reviews, see: (a) Muetterties, E. L., Ed. "Transition Metal Hydrides"; Dekker: New York, 1971. (b) Kaesz, H. D.; Saillant, R. B. *Chem. Rev.* **1972**, *72*, 231. (c) Bau, R., Ed. "Transition Metal Hydrides"; American Chemical Society: Washington, DC, 1978. (d) Cotton, F. A.; Wilkinson, G. "Advanced Inorganic Chemistry", 4th ed.; Wiley: New York, 1980; Chapters 27 and 30.
(2) Lohr, L. L., Jr.; Lipscomb, W. N. *Inorg. Chem.* **1964**, *3*, 22.
(3) Fenske, R. F.; DeKock, R. L. *Inorg. Chem.* **1970**, *9*, 1053.
(4) Guest, M. F.; Hall, M. B.; Hillier, I H. *Mol. Phys.* **1973**, *25*, 629.
(5) Grima, J.; Chaplin, F.; Kaufmann, G. *J. Organomet. Chem.* **1977**, *129*, 221.
(6) Fonnesbech, N.; Hjortkjaer, J.; Johansen, H. *Int. J. Quantum Chem. Suppl. 2* **1977**, *12*, 95.
(7) Hood, D. M.; Pitzer, R. M.; Schaefer, H. F., III *J. Chem. Phys.* **1979**, *71*, 705.
(8) Janowicz, A. H.; Bergman, R. G. *J. Am. Chem. Soc.* **1982**, *104*, 352.
(9) For reviews on the Xα–SW method, see: (a) Slater, J. C. *Adv. Quantum. Chem.* **1972**, *6*, 1. (b) Johnson, K. H. *Ibid.* **1973**, *7*, 143. (c) Connolly, J. W. D. In "Semiempirical Methods of Electronic Structure Calculation. Part A: Techniques"; Segal, G. A., Ed.; Plenum Press: New York, 1977; pp 105–132. (d) Case, D. A. *Annu. Rev. Phys. Chem.* **1982**, *33*, 151.
(10) Eyermann, C. J. Ph.D. Dissertation, Miami University, Oxford, OH, 1981.
(11) For related publications, see: (a) Eyermann, C. J.; Chung-Phillips, A. *J. Chem. Phys.* **1984**, *81*, 1517. (b) Eyermann, C. J.; Chung-Phillips, A. *Inorg. Chem.* **1984**, *23*, 2025.
(12) Kang, H.; Mauldin, C. H.; Cole, T.; Slegeir, W.; Cann, K.; Pettit, R. *J. Am. Chem. Soc.* **1977**, *99*, 8323.
(13) See, e.g.: Orchin, M. *Acc. Chem. Res.* **1981**, *14*, 259.
(14) McNeill, E. A.; Scholer, F. R. *J. Am. Chem. Soc.* **1977**, *99*, 6243.
(15) Evans, S.; Green, J. C.; Green, M. L. H.; Orchard, A. F.; Turner, D. W. *Faraday Discuss. Chem. Soc.* **1969**, *47*, 112.
(16) Guest, M. F.; Higginson, B. R.; Lloyd, D. R.; Hillier, I. H. *J. Chem. Soc., Faraday Trans. 2* **1975**, *71*, 902.
(17) Cradock, S.; Ebsworth, E. A. V.; Robertson, A. *J. Chem. Soc., Dalton Trans.* **1973**, 22.
(18) Blakney, G. B.; Allen, W. F. *Inorg. Chem.* **1971**, *10*, 2763.
(19) Sweaney, R. L. *Inorg. Chem.* **1982**, *21*, 752.
(20) Church, S. P.; Poliakoff, M.; Timney, J. A.; Turner, J. J. *J. Am. Chem. Soc.* **1981**, *103*, 7515.
(21) Symons, M. C. R.; Sweany, R. L. *Organometallics* **1982**, *1*, 834.
(22) Church, S. P.; Poliakoff, M.; Timney, J. A.; Turner, J. J. *Inorg. Chem.* **1983**, *22*, 3259.
(23) Sweany, R. L. *Inorg. Chem.* **1980**, *19*, 3512.
(24) Sweany, R. L. *J. Am. Chem. Soc.* **1981**, *103*, 2410.
(25) See, e.g.: Veillard, A. *Nouv. J. Chem.* **1981**, *5*, 599.
(26) See, e.g.: Veillard, A.; Dedieu, A. *Theor. Chim. Acta* **1983**, *63*, 339.

0002-7863/84/1506-7437$01.50/0

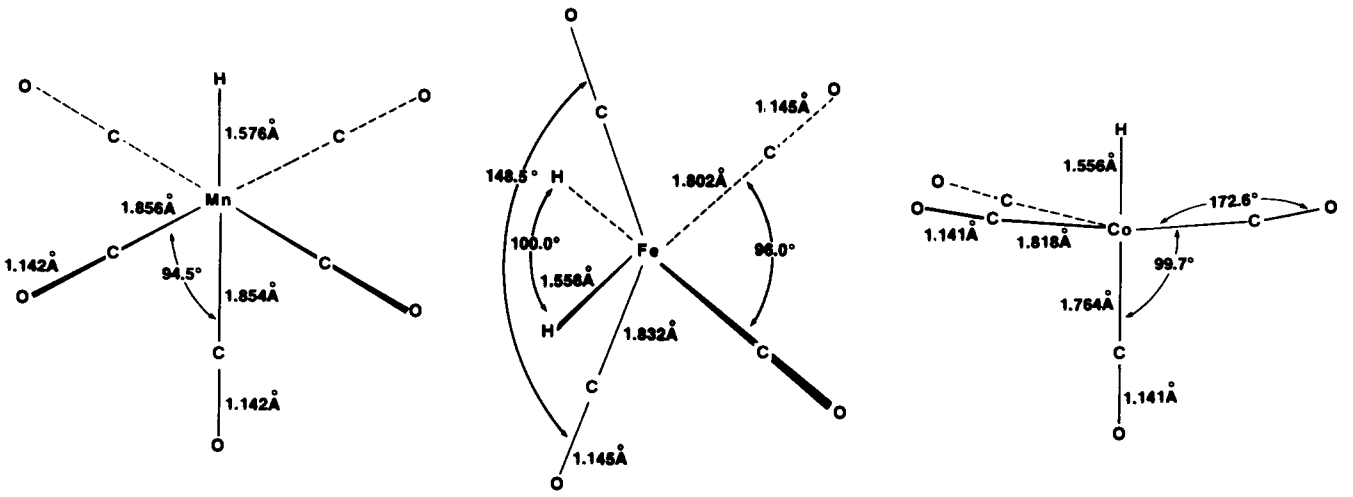

Figure 1. Geometries of $HMn(CO)_5$, $H_2Fe(CO)_4$, and $HCo(CO)_4$.

choice of theoretical method and the means of assessing the quality of the calculated energy levels.

It has been known for sometime that ab initio calculations for $HMn(CO)_5$, $H_2Fe(CO)_4$, and $HCo(CO)_4$, using SCF MOs expressed analytically as linear combinations of atomic orbitals (LCAO),[27,28] predict a HOMO that is metal–hydrogen (M–H) σ-bonding,[4,6,16] while the photoelectron spectra indicate the HOMO to be metal (M) 3d in character.[15-17] Although this discrepancy between calculations and observations is well documented, the current interpretation of the observed photochemistry of these complexes is based on the M–H σ-bonding HOMO deduced from the LCAO–MO method.[19,21,22]

For transition-metal complexes in general, it has also been known that the numerical Xα–SW method of Slater and Johnson is not only computationally more efficient than the ab initio LCAO–MO method but also yields better relative MO energies and spectroscopic quantities.[9] As for the specific hydride complexes $HMn(CO)_5$, $H_2Fe(CO)_4$, and $HCo(CO)_4$, we will demonstrate that the Xα–SW results for their IPs are in quantitative agreement (and transition energies in good agreement) with experimental data and that this agreement establishes the credibility of the Xα–SW orbital energy levels and orbital characteristics for use in the subsequent elucidation of their photoactive states.

Computational Details

The Xα–SW method has been described thoroughly in several reviews.[9] Details relevant to these calculations are given below.

Schematic drawings of the geometries[14] of $HMn(CO)_5$ (C_{4v}), $H_2Fe(CO)_4$ (C_{2v}), and $HCo(CO)_4$ (C_{3v}) are illustrated in Figure 1. In each case, the origin is set at the metal atom; the z axis is the symmetry axis; and the xz plane is a symmetry plane. The CO ligands are classified as cis and trans types depending on their locations relative to the H atom(s). Coordinates for the atoms and the center of outersphere (obtained as the valence-electron weighted average of all atomic coordinates) are available as supplementary material (Table S-I).

Schwarz's values[29] for the exchange parameter, α, were employed for the Mn, Fe, Co, C, and O atoms. An α value of 0.77725 was used for the H atom.[30] α values for the intersphere and outersphere regions were made equal and taken as the valence-electron weighted average of all atomic α values.

The initial molecular potential was generated from the superposition of SCF–Xα charge densities for the free metal (Mn, Fe, or Co), C, and O atoms. The 1s radial function of the free H atom was used for the H ligand. For the partial-wave expansion, spherical harmonics through $l = 4$ for the outersphere, $l = 2$ for the metal, $l = 1$ for the C and O, and $l = 0$ for the H regions were used.

Table I. Sphere Radii (bohrs)

region	$HMn(CO)_5$	$H_2Fe(CO)_4$	$HCo(CO)_4$
H	1.5246	1.5046	1.5088
metal	2.1557	2.1291	2.1309
C_{cis}	1.6131	1.6148	1.6122
O_{cis}	1.6314	1.6340	1.6310
C_{trans}	1.6134	1.6125	1.6073
O_{trans}	1.6314	1.6338	1.6307
outer	7.3605	7.4760	7.2820

The sphere radii were determined by the method of Norman.[31] Overlapping sphere radii were chosen nonempirically by using a scale factor of 0.88 over the atomic number sphere radii.[31] Values of the radii are shown in Table I.

A 9:1 ratio of old to new potentials for a given iteration was used as the starting potential for the next iteration in the SCF procedure. The metal 1s, 2s, 2p, 3s, and 3p and the C and O 1s orbitals were treated as core orbitals; i.e., their potentials were constructed by using only the charge densities inside the respective atomic spheres. The core energy levels were not frozen as they were computed in each iteration.

The ground-state orbital eigenvalues converged to better than ±0.0001 hartree. The virial theorem ratios based on the total kinetic (T) and potential (V) energies, $-2T/V$, were 1.0003 for both $HMn(CO)_5$ and $HCo(CO)_4$ and 1.0004 for $H_2Fe(CO)_4$. IPs and electronic transition energies were explicitly determined by using the converged SCF potentials for the ground state to start the requisite transition-state calculation.

In addition to the chosen set of sphere radii (set I), we also tried a second set (set II) for ground-state calculations and transition-state calculations of IPs.[10,11a] The radii in set II had the same size ratios for both the M–C spheres and the M–H spheres as those in set I, but their values were reduced to yield touching M–C spheres and ca. 30% C–O sphere overlap. Calculated results from set II were generally similar to those from set I, except for the magnitudes of IPs which were uniformly higher than the experimental values by about 2 eV. In view of the better IP values from set I, we decided to use set I throughout this study.

Ground-State Calculations

A ground-state Xα–SW calculation yields relative energies and sphere-charge distributions for the individual MOs and for the molecule as a whole. Numerical results from ground-state cal-

(27) For reviews on current theoretical methods, see: (a) Schaefer, H. F., III, Ed. "Methods of Electronic Structure Theory"; Plenum: New York, 1977. (b) Schaefer, H. F., III, Ed. "Applications of Electronic Structure Theory"; Plenum: New York, 1977.

(28) For reviews on MO applications to transition-metal complexes, see: (a) Mingos, D. M. P. *Adv. Organomet. Chem.* **1977**, *15*, 1. (b) Veillard, A.; Demuynck, J. In ref 27b, pp 187–222.

(29) (a) Schwarz, K. *Phys. Rev. B: Solid State* **1972**, *5*, 2466. (b) Schwarz, K. *Theor. Chim. Acta* **1974**, *34*, 225.

(30) Slater, J. C. *Int. J. Quantum Chem.* **1973**, *7S*, 533.

(31) (a) Norman, J. G., Jr. *J. Chem. Phys.* **1974**, *61*, 4630. (b) Norman, J. G., Jr. *Mol. Phys.* **1976**, *31*, 1191.

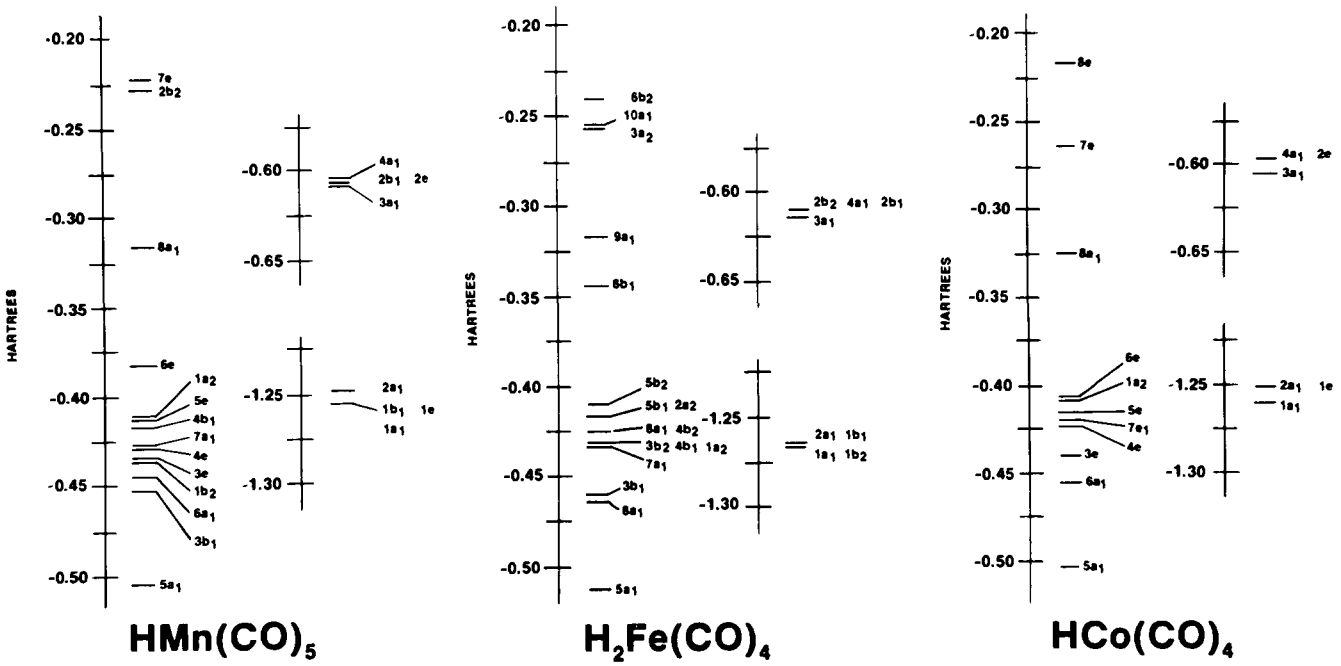

Figure 2. Valence energy level diagrams for $HMn(CO)_5$, $H_2Fe(CO)_4$, and $HCo(CO)_4$. The energy levels correspond to the Xα–SW orbital eigenvalues as defined in ref 9.

culations of the chosen complexes are provided as supplementary material (Tables S-II, S-III, and S-IV).

A synopsis of the valence MOs (Table S-II), with respect to their relative energies, is presented in Figure 2. In each diagram the MOs can be conveniently grouped into three regions according to their energies and characters. The MOs at ca. -1.25 and -0.60 hartrees are essentially the unperturbed CO 3σ and CO 4σ orbitals, respectively. MOs between -0.55 and -0.35 hartrees can be classified as M–C σ-bonding orbitals formed from metal orbitals and the CO 5σ orbitals, and as those derived principally from the CO 1π orbitals. Finally, the upper-valence MOs, located between -0.35 and -0.20 hartrees, are the M–H σ-bonding and the M 3d orbitals. Note especially that the HOMO in each complex is M 3d in character.

Ionization Potentials

Experimental and calculated IPs of the chosen complexes, corresponding to upper valence MOs of M 3d and M–H σ characters, are given in Table II. The orbital assignments were deduced from experimental band intensities and comparison with the photoelectron spectra of binary metal carbonyls.[15-17] Note that the M 3d orbitals were assigned *lower* IPs than the M–H σ orbital(s); i.e., IP(M–H) > IP(M 3d). Previous ab initio LCAO–MO calculations[4,6,16] predicted exactly the reverse trend when Koopmans' theorem (KT)[32] was invoked. The outcome could be partially explained by the failure of KT to properly account for orbital relaxation in the ionized species, especially for those centered on the metal.[33] When the ΔSCF method was used to remedy this situation, the relative magnitudes of IPs became rather poor,[16] owing to a neglect of correlation energy difference between the ionized and neutral species.

The Xα–SW method is known to incorporate some electron correlation; in addition, Slater's transition-state method allows for orbital relaxation.[9] These advantages manifest themselves markedly in the calculated IPs of transition-metal compounds.[34] A cursory examination of the Xα–SW values in Table II reveals that not only the experimental assignments are confirmed [IP(M–H) > IP(M 3d)] but also the numerical agreement is nearly quantitative (standard deviation 0.4 eV).

Table II. Ionization Potentials (eV)

orbital	type	exptl[a]	Xα–SW	KT[b]	ΔSCF[c]
		$HMn(CO)_5$			
7e	3d	8.85	8.69	12.2	8.2
$2b_2$	3d	9.14	8.79	12.3	8.6
$8a_1$	Mn–H	10.55	11.45	10.4	8.4
		$H_2Fe(CO)_4$			
$6b_2$	3d	9.65	9.17	14.4	9.2
$10a_1$	3d	9.65	9.77	14.2	
$3a_2$	3d	9.65	9.79	14.5	9.4
$9a_1$	Fe–H	10.95	11.16	11.3	9.1
$6b_1$	Fe–H	11.30	11.91	10.8	9.1
		$HCo(CO)_4$			
8e	3d	8.90	8.48	10.7	
7e	3d	9.90	10.09	14.4	
$8a_1$	Co–H	11.50	11.67	10.6	

[a] References 15–17. [b] References 4 and 6. [c] Reference 16.

The excellent Xα–SW IPs, calculated via transition-state approach by using the ground-state potential, infer that the ground-state Xα–SW MOs are of good quality. On that basis, we conclude that the HOMO in each complex is indeed M 3d in character and not M–H σ as has been proposed by a number of workers.

Electronic Spectra

$HMn(CO)_5$. The interpretation of electronic absorption spectra of d^6 $LM(CO)_5$ complexes (M = Mn or Re; L = H, Cl, Br, or I) has attracted much attention.[18,22,35-38] Thus far, the assignment of an observed band to a given orbital transition has depended upon observed band intensities and energy-level diagrams generated by simple qualitative arguments on the extent of metal–ligand interactions.

The experimental electronic transition energies for $HMn(CO)_5$, based on the vapor-phase spectrum,[18] are given in Table III. The

(32) Koopmans, T. *Physica* **1933**, *1*, 104.
(33) See, e.g.: Calabro, D. C.; Lichtenberger, D. L. *Inorg. Chem.* **1980**, *19*, 1732.
(34) See, e.g.: Bursten, B. E.; Jensen, J. R.; Gordon, D. J.; Treichel, P. M.; Fenske, R. F. *J. Am. Chem. Soc.* **1981**, *103*, 5226.
(35) Gray, H. B.; Billig, E.; Wojcicki, A.; Farona, M. *Can. J. Chem.* **1963**, *41*, 1281.
(36) Beach, N. A. Ph.D. Dissertation, Columbia University, New York, NY, 1967.
(37) McLean, R. A. N. Ph.D. Dissertation, Bristol University, Bristol, England, 1969.
(38) McLean, R. A. N. *J. Chem. Soc., Dalton Trans.* **1974**, 1568.

Table III. Electronic Transition Energies ($\times 10^3$ cm^{-1})[a]

	exptl[b]	transition[c]	Xα–SW[d]
$HMn(CO)_5$	~34.5 (0.1)	$7e \rightarrow 9a_1$	35.0
		$7e \rightarrow 10a_1$	37.5
	46.7 (0.75)	$7e \rightarrow 8e$ (CO 2π)	38.0
		$7e \rightarrow 3b_2$ (CO 2π)	39.0
		$7e \rightarrow 9e$ (CO 2π)	41.0
		$7e \rightarrow 11a_1$ (CO 2π)	41.3[e]
	51.3 (1.0)	$7e \rightarrow 5b_1$ (CO 2π)	45.5
		$7e \rightarrow 10e$ (CO 2π)	45.7[e]
		$7e \rightarrow 6b_1$ (Mn 3d)	45.2[e]
		$7e \rightarrow 12a_1$ (Mn 3d)	45.6[e]
		$7e \rightarrow 11e$ (CO 2π)	47.8[e]
$HCo(CO)_4$	44.0	$8e \rightarrow 9a_1$	36.0
	~53.4	$8e \rightarrow 9e$ (CO 2π)	37.8
		$8e \rightarrow 10$ e (CO 2π)	40.7
		$8e \rightarrow 10a_1$	49.4
		$8e \rightarrow 11a_1$	75.9

[a] 1000 cm^{-1} = 4.556 × 10^{-3} hartree. [b] Reference 18 and 19. Relative band intensities are given in parentheses. Only singlet → singlet spin transitions are observed. [c] All transitions are orbitally allowed. The HOMO for $HMn(CO)_5$, 7e, is Mn 3d in character. The HOMO for $HCo(CO)_4$, 8e, is Co 3d in character. The character of a virtual orbital is given in parentheses; however, see text concerning $9a_1$ and $10a_1$ of $HMn(CO)_5$ and $9a_1$ of $HCo(CO)_4$. [d] Spin-restricted transition-state calculations. Both singlet → singlet and singlet → triplet spin components are included. [e] Transition energy is estimated on the basis of the relaxation energy obtained from a similar transition which has already been explicitly calculated and listed in the table.

bands at 34.5 × 10^3 and 51.3 × 10^3 cm^{-1} are best described as shoulders on the dominant absorption at 46.7 × 10^3 cm^{-1}. Those at 46.7 × 10^3 and 51.3 × 10^3 cm^{-1} were unambiguously assigned to transitions involving metal-to-ligand charge transfer (MLCT); i.e., Mn → CO 2π transitions.[18,36-38] The origin of the band at ca. 34.5 × 10^3 cm^{-1} is less obvious. This weak low-energy band was initially attributed to a ligand-field (LF) transition, the so-called "d → d" transition.[35] Later it was reassigned as MLCT, Mn → CO 2π, where the CO 2π orbitals were taken to be noninteracting with respect to Mn.[18] Finally, this latter assignment was refuted on intensity grounds and a new proposal was made that the band at ca. 34.5 × 10^3 cm^{-1} belonged to a transition from a Mn 3d orbital to a Mn–H σ-antibonding (σ^*) orbital with some CO 2π character.[38]

The Xα–SW electronic transition energies for $HMn(CO)_5$, corresponding to transitions from the HOMO, 7e, to certain low-lying virtual orbitals, are also presented in Table III. The assignment of specific transitions to an observed band is made according to the ordering of the calculated transition energies and the character of the virtual orbitals involved. Most virtual orbitals are very diffuse. To assess the character of a virtual orbital, we resort to orbital sphere charges and contours. For this reason, contour plots for the $8a_1$ and 7e MOs and the $9a_1$, $10a_1$, 8e, 9e, 10e, and 11e virtual orbitals are presented in Figure 3 to facilitate discussion.

The Xα–SW values in Table III have been determined by spin-restricted transition-state calculations; thus, they correspond to weighted averages of the singlet → singlet and singlet → triplet spin components for a given orbital transition. Because the triplet state is lower in energy than the singlet state, the Xα–SW values are lower than the observed transition energy for a singlet → singlet spin excitation. Consequently, the Xα–SW values assigned to the MLCT transitions are about 5 × 10^3 cm^{-1} lower than the observed values of 46.7 × 10^3 and 51.3 × 10^3 cm^{-1}. A similar shift has been previously reported for Xα–SW calculations on the MLCT transitions in $Cr(CO)_6$.[39]

The attenuated intensity of the MLCT band at 46.7 × 10^3 cm^{-1} can be qualitatively understood by the ca. 10–20% Mn 3d character of $3b_2$ and 9e. Excitations from 7e, which is principally

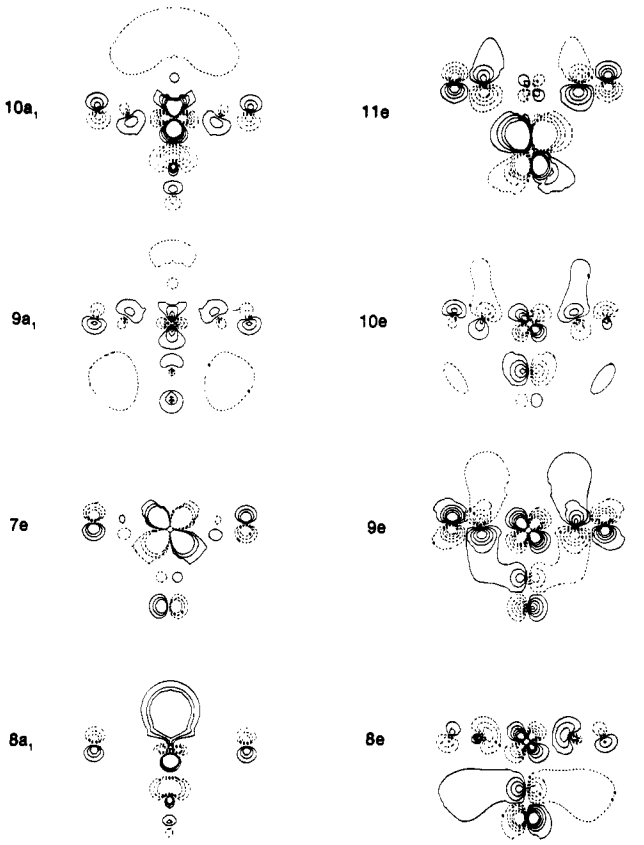

Figure 3. Selected orbital contour plots on the *xz* plane of $HMn(CO)_5$. The contour values in bohr$^{-2/3}$, starting from the outermost, are as follows: ±0.050, ±0.075, and ±0.100 for $8a_1$ and 7e; ±0.025, ±0.050, ±0.075, and ±0.100 for $9a_1$, $10a_1$, 10e, and 11e; ±0.025, ±0.050, ±0.075, ±0.100, and ±0.125 for 8e and 9e.

Mn 3d, into these orbitals will be in part a "d → d" transition for which the intensity is usually less than that for a MLCT transition.[38] As for the transition at 51.3 × 10^3 cm^{-1}, the $5b_1$, 10e, and 11e orbitals are almost entirely CO 2π with only a minimal amount of Mn 3d, exemplified by the contours of 11e in Figure 3. These orbitals are therefore expected to give the most intense MLCT absorptions in agreement with experimental intensities.

As previously noted, there is some controversy on the nature of the low-energy absorption at ca. 34.5 × 10^3 cm^{-1} in $HMn(CO)_5$. Xα–SW calculations suggest that $9a_1$, $10a_1$, and 8e are important in interpreting this portion of the spectrum. The sphere-charge distributions indicate that these orbitals are extremely diffuse, with more than 65% of the charge in the intersphere and extramolecular regions. The latter feature makes the conventional orbital characterization virtually impossible.

The contours around the equatorial COs in the 8e show CO 2π contours with some admixture of CO 5σ. Those around the axial CO are unambiguously CO 2π. The 7e → 8e transition, calculated at 38.0 × 10^3 cm^{-1}, is therefore identified as a MLCT transition; however, it will be only moderately intense due to the adulteration of the CO 2π character in the equatorial positions.

In $9a_1$ and $10a_1$, the contours around the equatorial COs are again CO 2π in appearance. Yet, these COs are basically noninteracting with respect to Mn because of a near symmetry incompatibility between the Mn $3d_{z^2}$ and the equatorial C $2p_z$ orbitals. Contours between Mn and the axial CO show Mn–C σ in $9a_1$ and Mn–C σ^* in $10a_1$. With respect to the Mn–H interaction, both orbitals display σ^* features in accord with the previous proposal[38] of a Mn 3d → Mn–H σ^* transition for the band at ca. 34.5 × 10^3 cm^{-1}. (It is conceivable that $9a_1$ and $10a_1$ are the respective antibonding counterparts of the Mn–H σ-bonding orbitals $7a_1$ and $8a_1$; e.g., compare $8a_1$ to $10a_1$ in Figure 3.)

(39) Johnson, J. B.; Klemperer, W. G. *J. Am. Chem. Soc.* **1977**, *99*, 7132.

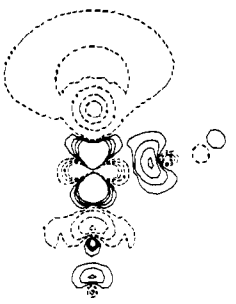

Figure 4. Orbital contour plot on the *xz* plane of $HCo(CO)_4$ for $9a_1$. The contour values in $bohr^{-2/3}$, starting from the outermost, are ±0.025, ±0.050, ±0.075, and ±0.100.

Existing spectroscopic data on the high-energy absorptions in d^6 hexacarbonyls and other complexes have shown that the MLCT bands involving COs noninteracting to the metal are usually very intense.[40] For $HMn(CO)_5$ the low-energy band around 34.5×10^3 cm^{-1} is weak; hence, the $7e \rightarrow 9a_1$ and $7e \rightarrow 10a_1$ transitions are not expected to be MLCT dominant. This deduction is reasonable considering that the equatorial CO 2π contours in $9a_1$ and $10a_1$ are not particularly prominent, relative to the contours in the axial regions containing Mn, H, and the axial CO.

As $9a_1$ is more diffuse than $10a_1$ and therefore more difficult to characterize, our discussion on the nature of transitions for the observed low-energy band will thus focus on the $7e \rightarrow 10a_1$ transition. In view of the generally diffuse nature of $10a_1$, the ca. 20% Mn 3d character found in $10a_1$ again suggests that the transition is in part a "d → d" transition, which would then account for the relatively low intensity of the experimental band.

The calculated energies of 35.0×10^3 and 37.5×10^3 cm^{-1} for the $7e \rightarrow 9a_1$ and $7e \rightarrow 10a_1$ transitions are respectively 0.5×10^3 and 3.0×10^3 cm^{-1} higher than the observed 34.5×10^3 cm^{-1}. These deviations could be the net result of overestimation in the orbital energies of $9a_1$ and $10a_1$ and underestimation (ca. 5×10^3 cm^{-1}) due to the singlet → triplet component in the transition-state calculation. For example, the Xα–SW IP for $8a_1$ in Table II is 0.9 eV (equivalent to 7.2×10^3 cm^{-1}) higher than the experimental value, which infers that the energy attributed to $8a_1$ is too low. As a result, the energy for its antibonding partner, $10a_1$, becomes too high, and the associated transition energy for $7e \rightarrow 10a_1$ likewise becomes too high. The same consideration may be applied to the bonding and antibonding pair of $7a_1$ and $9a_1$ and the $7e \rightarrow 9a_1$ transition.

In summary, the Xα–SW transition-state calculations confirm the latest empirical assignments for the electronic absorption spectrum of $HMn(CO)_5$,[38] including the low-energy absorption band at 34.5×10^3 cm^{-1} as predominantly a Mn 3d → Mn–H σ^* transition.

$HCo(CO)_4$. A summary of the UV–vis spectrum of $HCo(CO)_4$ in an argon matrix[19] is given in Table III. The lowest energy absorption at 44.0×10^3 cm^{-1} (227 nm) is a shoulder on a very intense band at 53.4×10^3 cm^{-1} (187 nm). Attempts to observe weak transition to shorter wavelengths of 44.0×10^3 cm^{-1} were unsuccessful.[19]

Results of Xα–SW transition-state calculations to account for these transitions of $HCo(CO)_4$ are also listed in Table III. Our discussion primarily focusses on the assignment of the absorption at 44.0×10^3 cm^{-1}.

Previously, this 44.0×10^3 cm^{-1} band was attributed to a H to Co charge transfer, or a ligand-to-metal charge transfer (LMCT), transition.[19] This assignment was based on intensity arguments and ab initio LCAO–MO calculations.[19,25] In the following we propose an alternative assignment.

The photoelectron spectrum[17] of $HCo(CO)_4$ and our Xα–SW calculations both indicate that the HOMO, 8e, is Co 3d in character. If this is the case, the band cannot be LMCT but is more likely to be LF or MLCT. An inspection of the contours for the LUMO of $HCo(CO)_4$, $9a_1$ in Figure 4, reveals that this virtual orbital has considerable Co and ligand character. We therefore believe that the lowest energy electronic transition, 8e → $9a_1$, is best described as an intermediate between LF and MLCT transitions.

Two empirical facts support the Xα–SW assignment of the $8e \rightarrow 9a_1$ transition to the 44.0×10^3 cm^{-1} band. First, the band has large intensity ($\epsilon > 5500$, where ϵ is the molar decadic extinction coefficient),[19] which is larger than, for example, LF transition observed for $LCr(CO)_5$ ($\epsilon \approx 1400$).[41a] The clear admixture of the Co $3d_{z^2}$ orbital with the ligand orbitals in $9a_1$ suggests that the relatively high intensity observed for the band is due to the MLCT component in the proposed transition. On the other hand, the observed intensity is expected to be lower than the intensity of a "pure" MLCT transition owing to the large percentage of LF character in the transition. Second, the presence of the LF component in the transition is the reason for failing to observe any "pure" weak LF transitions to shorter wavelengths of 44.0×10^3 cm^{-1}.

It is worthwhile to note the similarity of the LUMO $9a_1$ of $HCo(CO)_4$ in Figure 4 and the two lowest lying virtual orbitals, $9a_1$ and $10a_1$, of $HMn(CO)_5$ in Figure 3. The similarity infers two general (and related) features pertaining to the lowest energy electronic transition in a simple mononuclear monohydride complex. First, the LUMO involves considerable mixing of metal and ligand atomic orbitals. Second, a transition from a HOMO of metal 3d character to a LUMO of this particular nature necessarily entails both LF "d → d" and MLCT character.

We now turn to the high-intensity band at 53.4×10^3 cm^{-1}, which was considered somewhat in doubt because of its proximity to the lower wavelength limit of the spectrometer.[19] On the basis of intensity consideration and Xα–SW calculations, the MLCT transitions 8e → 9e and 8e → 10e, as well as the next two transitions 8e → $10a_1$ and 8e → $11a_1$, may be tentatively assigned to this band. Finally, it should be mentioned that the marked differences between the Xα–SW values and the observed values (44.0×10^3 and 53.4×10^3 cm^{-1}) may be attributed to reasons similar to those described in the preceding section on $HMn(CO)_5$.

Photochemistry

Recent studies on the photochemistry of transition-metal hydride complexes have established some apparently fundamental types of photochemical reactions.[41] For a complex containing only a single M–H bond, the non-hydrogen ligand photodissociation is definitely favored, but a photoinduced M–H bond homolysis is also observed. For complexes with two or more M–H bonds, photolysis induces elimination of H_2 irrespective of how thermally resistant the complex is to H_2 dissociation.

An important application of our quantitative study of the electronic structure of the chosen complexes is to provide a consistent and rigorous theoretical interpretation to the observed photochemistry. In the following discussion we use $HMn(CO)_5$ and $HCo(CO)_4$ as models for the monohydrides and $H_2Fe(CO)_4$ as a model for the dihydrides.

$HMn(CO)_5$. The photochemistry of $HMn(CO)_5$ has been carefully examined lately.[20-22,42] In the previous discussion on the electronic spectrum of $HMn(CO)_5$, we have assigned the lowest energy transitions to the orbital transitions $7e \rightarrow 9a_1$, $7e \rightarrow 10a_1$, and $7e \rightarrow 8e$. The $7e \rightarrow 8e$ transition is MLCT in character and therefore is not expected to lead to photodissociation of any ligand. Unfortunately, the diffuse nature of $9a_1$ precludes any definitive a priori statement on what effect a $7e \rightarrow 9a_1$ transition would have on $HMn(CO)_5$. The better understood transition, $7e \rightarrow 10a_1$, may be considered LF in character as it corresponds to a transition from a Mn 3d orbital to an orbital with relatively predominant Mn 3d character. Both $9a_1$ and $10a_1$ are Mn–H σ^*.

Experimentally, irradiation of $HMn(CO)_5$ with 229-nm light yields the dissociation of CO and the formation of $HMn(CO)_4$.[42] The dissociative loss of CO observed for $HMn(CO)_5$ can be partially justified by a $7e \rightarrow 10a_1$ transition because $10a_1$ is also

(40) Beach, N. A.; Gray, H. B. *J. Am. Chem. Soc.* **1968**, *90*, 5713.
(41) For recent reviews on photochemistry, see: (a) Geoffroy, G. L.; Wrighton, M. S. "Organometallic Photochemistry"; Academic: New York, 1979. (b) Geoffroy, G. L. *Prog. Inorg. Chem.* **1979**, *27*, 123.
(42) Rest, A. J.; Turner, J. J. *J. Chem. Soc., Chem. Commun.* **1969**, 375.

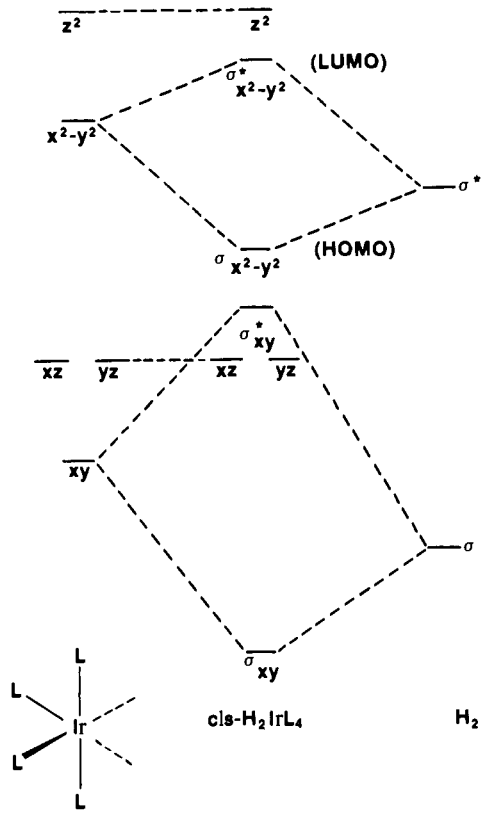

Figure 5. Qualitative energy-level diagram for *cis*-H_2IrL_4 (based on: Geoffroy, G. L.; Pierantozzi, R. *J. Am. Chem. Soc.* **1976**, *98*, 8054, Figure 3).

Mn–C σ^* in character (Figure 4) and population of $10a_1$ will weaken the metal–axial CO linkage.

In summary, the $7e \rightarrow 10a_1$ transition can conceivably cause two photochemical reactions: first, a homolysis of the Mn–H bond, and second, the dissociative loss of CO. From all information available to date, the latter process appears more favorable. Even when Mn–H bond cleavage does occur,[20] the quantum yield is small, indicating a low efficiency for the available reaction pathways.

$HCo(CO)_4$. Two reactions occur when $HCo(CO)_4$ is photolyzed in a matrix: Co–H bond homolysis and CO dissociation.[19] The CO photodissociation predominates by approximately eightfold over Co–H bond cleavage unless the former process is suppressed by the use of a CO matrix. The observed photochemistry has been previously interpreted on the basis of a Co–H $\sigma \rightarrow$ Co–H σ^* orbital transition.[19,25]

In view of the Xα–SW result for the lowest energy electronic transition of $HCo(CO)_4$, $8e \rightarrow 9a_1$, we offer a different explanation. The transition is best described as both LF and MLCT in character. The HOMO is predominantly the E symmetry combination of the Co $3d_{x^2-y^2}$ and Co $3d_{xy}$ atomic orbitals. The contours for the LUMO in Figure 4 indicate that there are both Co–CO σ^* and Co–H σ^* interactions. An electronic transition from the HOMO to the LUMO could therefore directly lead to CO photodissociation or Co–H bond homolysis. Such a transition is completely consistent with the observed photochemistry; however, as in the case of $HMn(CO)_5$, we are unable to predict which process is more favorable.

$H_2Fe(CO)_4$. The photochemistry of a number of dihydride complexes has been amply explored,[25,43-46] including that of $H_2Fe(CO)_4$.[24,26] A strong emphasis has been placed on the d^6 H_2ML_4 complexes (M = Ru or Ir; L = CO or PH_3). For *cis*-H_2IrL_4 complexes, exposure to light invariably results in the elimination of H_2 and the formation of a very reactive IrL_4 species.[8] Two different excited states have been proposed to account for this observed chemistry.

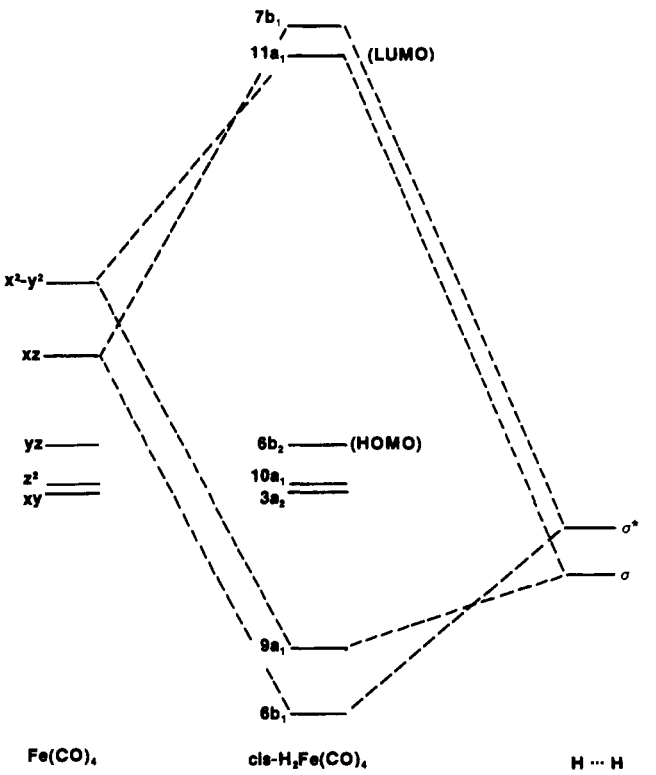

Figure 6. Simple orbital interaction diagram for *cis*-$H_2Fe(CO)_4$. The diagram intends to show the parentage of the $H_2Fe(CO)_4$ orbitals. Energy-level spacings are postulated. Geometries of $Fe(CO)_4$ and H···H correspond to those of the respective moieties in $H_2Fe(CO)_4$. The ordering of energy levels for $Fe(CO)_4$ is deduced from the valence energy levels and sphere-charge distributions for $H_2Fe(CO)_4$ in Table S-II.

One of the excited states is based on the qualitative energy-level diagram for *cis*-H_2IrL_4 and related d^6 octahedral complexes shown in Figure 5, as proposed by Geoffroy and Pierantozzi.[44] In this diagram, the HOMO $\sigma_{x^2-y^2}$ is Ir–H σ, which is formed by the interaction of Ir $3d_{x^2-y^2}$ of IrL_4 with σ^* of H_2. The LUMO is $\sigma^*_{x^2-y^2}$, shown as both Ir–H σ^* and H–H σ^*. A transition from the HOMO to the LUMO has been postulated to lead into the active excited state for the elimination of H_2 from H_2IrL_4.

Next, consider *cis*-$H_2Fe(CO)_4$ in this study, which is also a d^6 H_2ML_4 complex. Its photoelectron spectrum and Xα–SW IPs shown in Table II suggest to us that an energy-level diagram different from that in Figure 5 is required. First, the HOMO does not represent the Fe–H σ-bond but is basically a Fe 3d orbital. Second, the σ and σ^* orbitals of H_2 in Figure 5 are likely to be too positive in energy. The statement is based on our recent finding[11a] of a value of −0.33 for the atomic charge of each H ligand, Q^H, in $H_2Fe(CO)_4$ by using the projected Xα method.[47] This Q^H value implies that the H ligands are more electronegative in transition-metal dihydrides than what is indicated by the H_2 energy levels in Figure 5. For comparison, a simple orbital interaction diagram is postulated in Figure 6 to illustrate the parentage of the Xα–SW upper valence MOs and the two lowest lying virtual orbitals. (Note that the molecular coordinate systems in Figures 5 and 6 are different.) Contour plots for the $6b_1$, $9a_1$, $11a_1$, and $7b_1$ orbitals relevant to this discussion are presented in Figure 7.

In Figure 6, the H···H levels have been shifted to the point where the most stable Fe–H σ-bonding MO, $6b_1$, is formed by overlapping Fe $3d_{xz}$ with H···H σ^*. The other Fe–H σ-bonding MO, $9a_1$, is higher in energy and is generated by an overlap

(43) Geoffroy, G. L.; Gray, H. B.; Hammond, G. S. *J. Am. Chem. Soc.* **1975**, *97*, 3933.
(44) Geoffroy, G. L.; Pierantozzi, R. *J. Am. Chem. Soc.* **1976**, *98*, 8054.
(45) Geoffroy, G. L.; Bradley, M. G. *Inorg. Chem.* **1977**, *16*, 744.
(46) Geoffroy, G. L.; Bradley, M. G. *Inorg. Chem.* **1978**, *17*, 2410.
(47) Bursten, B. E.; Fenske, R. F. *J. Chem. Phys.* **1977**, *67*, 3138.

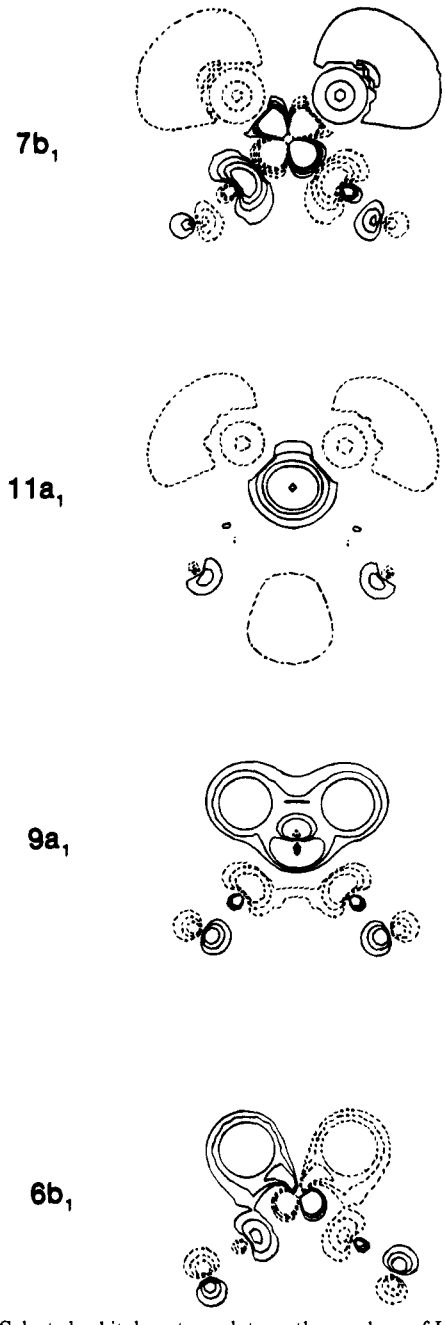

Figure 7. Selected orbital contour plots on the xz plane of $H_2Fe(CO)_4$. The contour values in $bohr^{-2/3}$, starting from the outermost, are as follows: ±0.050, ±0.075, and ±0.100 for $6b_1$ and $9a_1$; ±0.025, ±0.050, ±0.075, and ±0.100 for $11a_1$ and $7b_1$.

between Fe $3d_{x^2-y^2}$ (with some Fe $3d_{z^2}$ character expected)[48] and H···H σ. If this bonding scheme is correct, the LUMO will be the antibonding counterpart of $9a_1$; indeed, the orbital assigned as the LUMO, $11a_1$, is antibonding with respect to Fe–H interaction but is "bonding" between the two H ligands. (See Figure 7 for the orbital contours of the bonding and antibonding pairs: $6b_1$ vs. $7b_1$ and $9a_1$ vs. $11a_1$.) The last point, concerning the H···H interaction in the LUMO $11a_1$, reflects a critical difference between the two LUMOs, $\sigma^*_{x^2-y^2}$ in Figure 5 and $11a_1$ in Figure 6.

To repeat for emphasis, while both Figures 5 and 6 depict the LUMO to be M–H σ^*, it is H–H σ^* in $\sigma^*_{x^2-y^2}$ but H···H σ in $11a_1$. Experimentally, H_2 photodissociation is found to proceed via a *concerted* mechanism; thus, a LF transition into a virtual orbital such as the $11a_1$ of $H_2Fe(CO)_4$ favoring H_2 formation (H–H σ) would be more reasonable than a LF transition into a $\sigma^*_{x^2-y^2}$ orbital that favors the dissociation of two H atoms (H–H σ^*). For this reason, we believe that the orbital interaction diagram in Figure 6 serves a better model for the H_2 dissociation in a d^6 H_2ML_4 complex.[41]

A second excited state which could lead to H_2 photodissociation comes from a MLCT transition.[43] In such an excited state the metal becomes electron deficient and stabilization could be achieved via a reductive elimination of H_2. This hypothesis is again consistent with the negatively charged H ligands (Q^H = -0.33) in $H_2Fe(CO)_4$:[11a] donation of the excess charge on the H ligands to stabilize the metal would weaken the M–H bond and could subsequently lead to H_2 dissociation. Precedence for such a mechanism has been found in a study on several dialkyl Pt(II) complexes where one-electron oxidation of the complex to a Pt(III) intermediate appears to promote the reductive elimination of alkyl radicals.[49]

Presently, it is not possible to justifiably favor one excited state over the other (LF vs. MLCT) for the photodissociation of H_2 from a d^6 H_2ML_4 complex. In theory, either a LF transition (involving M–H σ^* as LUMO) or a MLCT transition could induce a facile elimination of H_2. Experimentally, the electronic spectra of H_2IrL_4 complexes are poorly resolved,[41] precluding assignment of the first absorption band at ca. 27×10^3 cm^{-1} (370 nm) as either a LF or a MLCT band. For $H_2Fe(CO)_4$, we favor an excited state generated by a LF transition since it results in the direct population of a Fe–H σ^* (but H···H σ) virtual orbital.

From the preceding discussion, it is obvious that a priori predictions concerning the photochemical behavior of hydride complexes are not currently feasible. At best, experimental data can be combined with a one-electron model to help piece together a possible excited state or sequence of events which may explain the observed photochemistry.[48] Therefore, while the excited states postulated for $HMn(CO)_5$, $HCo(CO)_4$, and $H_2Fe(CO)_4$ are consistent with experimental data, they are not the only possibilities.

Acknowledgment. We are indebted to Professor S. Doniach, Professor H. Schlosser, and Dr. D. K. Misemer for their valuable assistance with the Xα–SW programs. We also thank Professor J. G. Norman, Jr., for a very helpful correspondence. The work was supported in part by a grant from the Faculty Research Committee of Miami University.

Registry No. $HMn(CO)_5$, 16972-33-1; $H_2Fe(CO)_4$, 12002-28-7; $HCo(CO)_4$, 16842-03-8.

Supplementary Material Available: Tables S-I (geometric coordinates), S-II (valence energy levels and sphere charge distributions), S-III (core energy levels), and S-IV (total energies and sphere charges) for $HMn(CO)_5$, $H_2Fe(CO)_4$, and $HCo(CO)_4$ (5 pages). Ordering information is given on any current masthead page.

(48) See, e.g.: Balazs, A. C.; Johnson, K. H.; Whiteside, G. M. *Inorg. Chem.* **1982**, *21*, 2162.

(49) Chen, J. Y.; Kochi, J. K. *J. Am. Chem. Soc.* **1977**, *99*, 1450.